N90-11603
234869
p. 45

T · H · E
OHIO
STATE
UNIVERSITY

Constitutive Parameter Measurements of Lossy Materials

A. Dominek and A. Park

The Ohio State University
ElectroScience Laboratory

Department of Electrical Engineering
Columbus, Ohio 43212

Semi-Annual Report 721837-1
Grant No. NAG3-1000
September 1989

National Aeronautics and Space Administration
Lewis Research Center
21000 Brookpark Rd.
Cleveland, Ohio 44135

(NASA-CR-183398) CONSTITUTIVE PARAMETER MEASUREMENTS OF LOSSY MATERIALS (Ohio State Univ.) 45 p
CSCL 20L
N90-11603
Unclas
G3/76 0234869

NOTICES

When Government drawings, specifications, or other data are used for any purpose other than in connection with a definitely related Government procurement operation, the United States Government thereby incurs no responsibility nor any obligation whatsoever, and the fact that the Government may have formulated, furnished, or in any way supplied the said drawings, specifications, or other data, is not to be regarded by implication or otherwise as in any manner licensing the holder or any other person or corporation, or conveying any rights or permission to manufacture, use, or sell any patented invention that may in any way be related thereto.

50272-101

REPORT DOCUMENTATION PAGE	1. REPORT NO.	2.	3. Recipient's Accession No.

4. Title and Subtitle
Constitutive Parameter Measurements of Lossy Materials

5. Report Date
September 1989

6.

7. Author(s)
A. Dominek and A. Park

8. Performing Org. Rept. No.
721837-1

9. Performing Organization Name and Address
The Ohio State University
ElectroScience Laboratory
1320 Kinnear Road
Columbus, OH 43212

10. Project/Task/Work Unit No.

11. Contract(C) or Grant(G) No.
(C)
(G) NAG3-1000

12. Sponsoring Organization Name and Address
National Aeronautics and Space Administration, Lewis Research Center
21000 Brookpark Rd.
Cleveland, OH 44135

13. Report Type/Period Covered
Semi-Annual Report

14.

15. Supplementary Notes

16. Abstract (Limit: 200 words)

The electrical constitutive parameters of lossy material are of interest here. A discussion of the NRL arch for lossy coatings is presented involving analytical analyses of the reflected field using GTD and PO. The actual values for these parameters can be obtained through a traditional "transmission" technique which is examined from an error analysis standpoint. Alternate sample geometries are suggested for this technique to reduce sample tolerance requirements for accurate parameter determination. The performance for one alternate geometry is given.

17. Document Analysis a. Descriptors

b. Identifiers/Open-Ended Terms

c. COSATI Field/Group

18. Availability Statement	19. Security Class (This Report)	21. No. of Pages
A. Approved for public release; Distribution is unlimited.	Unclassified	43
	20. Security Class (This Page) Unclassified	22. Price

(See ANSI-Z39.18) *See Instructions on Reverse* OPTIONAL FORM 272 (4-77) Department of Commerce

Contents

List of Figures iv

1 Introduction 1

2 NRL Arch 3

3 Material Parameter Extraction Using Waveguides 11

4 Partially Filled Waveguides 20

I Field Expansions 21

II Calculations and Measurements 23

5 Conclusions 37

PRECEDING PAGE BLANK NOT FILMED

List of Figures

2.1 Near field scattering from a strip. 4

2.2 Far field scattering for a plate with plane wave incidence. . 8

2.3 Measured (solid) and calculated (dashed) reflection coefficients for a 5" square planar sample of lossy magnetic material. 9

2.4 Measured (solid) and calculated (dashed) reflection coefficients for a 12" square planar sample of lossy magnetic material. 10

3.1 Normalized error for ϵ when S_{11} has a phase position error of .001" (solid) and .003" (dashed). The sample parameters are $\mu_r = (1.42, -j.8)$ and $\epsilon_r = (7.8, -j.17)$ with $d = .05$". Coaxial airline fixture. 16

3.2 Normalized error for ϵ when S_{11} has a phase position error of .001" (solid) and .003" (dashed). The sample parameters are $\mu_r = (1.42, -j.8)$ and $\epsilon_r = (7.8, -j.17)$ with $d = .05$". Rectangular waveguide fixture. 17

3.3 Normalized error for ϵ when S_{11} has a sample length error of $-.002$" (solid) and $+.002$" (dashed). The sample parameters are $\mu_r = (1.42, -j.8)$ and $\epsilon_r = (7.8, -j.17)$ with $d = .05$". Coaxial airline fixture. 18

3.4 Normalized error for ϵ when S_{11} has a sample length error of $-.002$" (solid) and $+.002$" (dashed). The sample parameters are $\mu_r = (1.42, -j.8)$ and $\epsilon_r = (7.8, -j.17)$ with $d = .05$". Rectangular waveguide fixture. 19

4.1 Partially filled waveguide geometries. 25

4.2 Waveguide regions. 26

4.3 Calculated S_{11} for $t = .2", .5", .7"$, and .9" in a X-band fixture (.4"x.9") when $\mu_r = (1.42, -j.8)$, $\epsilon_r = (7.8, -j.17)$ and $l = .3"$. 27

4.4 Calculated S_{21} for $t = .2", .5", .7"$, and .9" in a X-band fixture (.4"x.9") when $\mu_r = (1.42, -j.8)$, $\epsilon_r = (7.8, -j.17)$ and $l = .3"$. 28

4.5 Calculated S_{11} for $\epsilon_r = 2, 5, 8, 11$, and 14 in a X-band fixture (.4"x.9") when $\mu_r = (1., -j0.)$, $t = .1"$ and $l = .5"$. 29

4.6 Calculated S_{21} for $\epsilon_r = 2, 5, 8, 11$, and 14 in a X-band fixture (.4"x.9") when $\mu_r = (1., -j0.)$, $t = .1"$ and $l = .5"$. 30

4.7 Calculated error for a .002" air gap along the short wall for a rectangular guide with $\mu_r = (1.42, -j.8)$, $\epsilon_r = (7.8, -j.17)$ and $l = .3"$. 31

4.8 Measured and calculated S_{11} for a partially filled rectangular X-band guide with $t = .082"$. Geometry A. 32

4.9 Measured and calculated S_{21} for a partially filled rectangular X-band guide with $t = .082"$. Geometry A. 33

4.10 Illustration of X-band fixture used for material measurements. 34

4.11 Measured S_{11} for a partially filled rectangular X-band guide with $t = .082"$. Geometry B. 35

4.12 Measured S_{21} for a partially filled rectangular X-band guide with $t = .082"$. Geometry B. 36

Chapter 1

Introduction

Several techniques are available for the determination of constitutive material parameters. The technique of choice is dependent upon sample geometry, frequency range of interest and the relative range of parameter values. Some techniques involve the measurement of reflection and transmission of RF energy which then can be related to the properties of the geometry samples. Naturally, rigorous relationships have to exist between the measured quantities and the material parameters. The parameters which describe the materials electrically are the quantities permittivity (ϵ) and permeability (μ) which relate the electric and magnetic field intensities to their flux densities. Mathematically, this relationship is

$$\mathbf{D} = \epsilon \mathbf{E} \tag{1.1}$$

and

$$\mathbf{B} = \mu \mathbf{H}. \tag{1.2}$$

One common apparatus used for the acquisition of the specular reflection performance of lossy material samples is the NRL arch. The sample is usually a planar conductive panal coated with some material. Attempts

for parameter extraction are usually limited to just one parameter for a lossy material (usually non-magnetic). Two complex parameters have to be extracted if the material is magnetic.

An accepted measurement technique for constitutive parameter determination involves the reflection and transmission measurement of samples in an airline or waveguide fixture. This approach, unlike the NRL arch, has a known rigorous relationship between the measurable reflected-transmitted fields and the constitutive parameters. The practice is to completely fill the interior cross section of the fixture with the material for a given length. Simple expressions exists to obtain the desired parameters. Potential sources of error aside from related hardware limitations are sample dependent. The sample uniformity, geometry and position in the fixture can limit the accuracy of the desired parameter values.

Potential accuracy improvements in the parameter values are possible if alternate sample geometries are used. Requiring the sample to completely fill the cross section of the fixture requires a good fit between the sample and fixture walls. If the fit is not adequate the measured quantities do not correspond to the anticipated geometry. Introducing a known gap between the sample and a fixture wall may make a less sensitive requirement in the actual dimensions for the sample. This gain is offset by the increased complexity of the reflected and transmitted field solutions.

This report discusses and contains results for NRL arch measurements and waveguide fixture performances for completely and partially filled waveguides.

Chapter 2

NRL Arch

The NRL arch is simply a hardware configuration to acquire the reflection performance of material coatings. The term "reflection" refers to scattering between the transmit and receive horns which satisfies Snell's Law of Reflection (angle of incidence equals angle of reflection) from the surface of the material. This restriction is imposed for the following material to allow a description as accurate as possible of the scattered field without a great amount of complexity.

The scattering from a two dimensional geometry as shown in Figure 2.1 consists of three dominant mechanisms, i.e., two edge diffracted contributions and one specular contribution when viewed from a high frequency viewpoint (the dimension "w" is much larger than the incident wavelength). The direct coupling between the transmit and receive horns is ignored here. This field decomposition fails when the strip is electrically small. As the distance between the transmit-receive horns and the strip become large, it is easily shown that the reflected field can be represented by the edge diffracted fields alone. Large refers to the distance required to maintain a constant phase across the surface of the strip. An accepted distance, R, to achieve plane wave illumination (constant phase) is

$$R \geq 2\frac{W^2}{\lambda}. \tag{2.1}$$

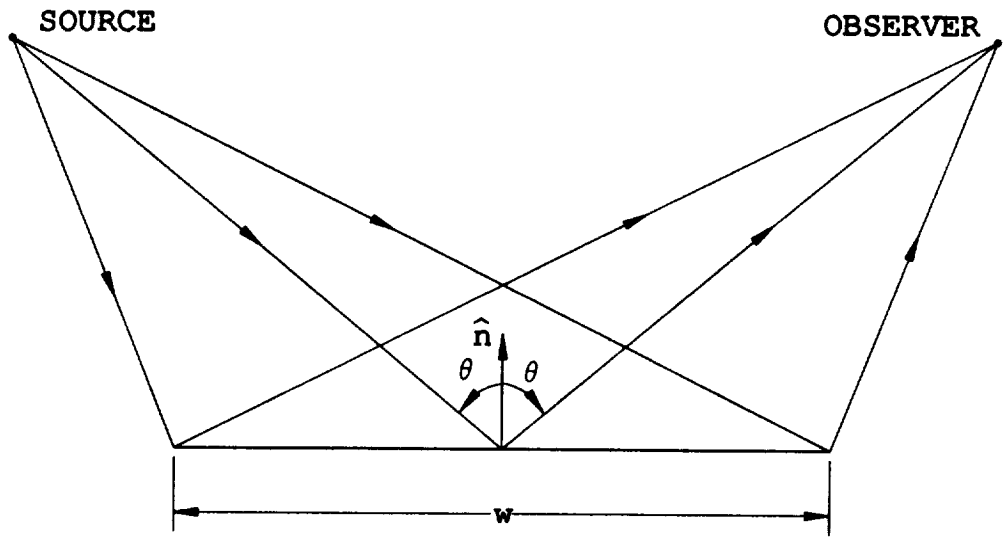

Figure 2.1: Near field scattering from a strip.

A detailed study of general bistatic scattering from a perfectly conducting strip has been done [1] which analytically and rigorously demonstrates the above described behavior. The significance of this analysis is that it demonstrates that the scattering from a planar surface which satisfies the reflection law can be represented as an edge diffracted field. However, the edge diffracted fields for plane wave incidence in the far field does simulate a reflected field when reflection law is satisfied.

The two dimensional strip can be extended into a three dimensional plate case when the other orthogonal plate dimension is electrically large. The transformation of two to three dimensional fields is given by

$$E_{3d} = \frac{L}{\sqrt{\lambda}} e^{j\frac{\pi}{4}} E_{2d} \tag{2.2}$$

and geometrically illustrated in Figure 2.2.

The principle plane physical optics (PO) approximation for the specular scattered planar plate of dimensions w by L with parallel polarization is

$$E^s = jR_s \cos\theta \frac{wL}{\lambda} \frac{e^{-jkr}}{r} \tag{2.3}$$

and with perpendicular polarization it is

$$E^s = -jR_h \cos\theta \frac{wL}{\lambda} \frac{e^{-jkr}}{r}. \tag{2.4}$$

The polarization designations are with respect to the electric field direction and the incident plane of incidence. The quantities $R_{s,h}$ are the Fresnel reflection coefficients for an infinite conducting planar surface with an uniform coating of material (thickness being t). The Fresnel reflection coefficients are

$$R_s = \frac{j\eta_r \cos\theta \tan(kt\cos\theta^t) - \cos\theta^t}{j\eta_r \cos\theta \tan(kt\cos\theta^t) + \cos\theta^t} \tag{2.5}$$

and

$$R_h = -\frac{j\eta_r \cos\theta^t \tan(kt\cos\theta^t) - \cos\theta}{j\eta_r \cos\theta^t \tan(kt\cos\theta^t) + \cos\theta} \tag{2.6}$$

where $\eta_r = \sqrt{\frac{\mu_r}{\epsilon_r}}$, $k = \sqrt{\mu_r \epsilon_r} k_o$ and $k_o \sin\theta = k \sin\theta^t$.

A more accurate approximation to the specular scattered field is given by GTD [2,3] based upon edge diffraction through accounting for the first order change in the reflection shadow boundary for material coating. The scattered field for parallel polarization is

$$E^s = \frac{-1}{2\pi} \left(\frac{1}{\cos\theta} - jR_s kw \cos\theta \right) L \frac{e^{-jkr}}{r} \tag{2.7}$$

and for perpendicular polarization it is

$$E^{s} = \frac{1}{2\pi}\left(\frac{1}{\cos\theta} - jR_h kw\cos\theta\right) L\frac{e^{-jkr}}{r}. \tag{2.8}$$

The first term in these expressions is a result of the discontinuity of the incident field.

Conceptually, parameter extraction for both ε and μ is possible when measurements for two different incident angles are performed. The two incident angles would have to be sufficiently different to insure the measurements to have their own unique character. Attempts have been made based upon PO approximations which have yielded poor results [4]. Such results would be valid only when the second term is the parenthesis of Equations (2.7) and (2.8) is dominant. The GTD approximation would potentially do better but the scattered field representation may not be rigorous enough if a surface wave is induced in the coating.

Arch measurements were performed for normal incidence upon planar coated metallic plates. The arch was configured with a single 2-18 GHz AEL horn 70" from the plates. Better performance can be obtained if two horns are used instead of one due to the input mismatch of broadband horns. The horn to horn return is up to 20 dB less than the mismatch return for a single horn at the higher frequencies. A septum is suggested to help minimize the coupling between the horns. A high gain horn will also provide greater sensitivity due to lower sidelobe levels to sense the nearby environment.

Figures 2.3 and 2.4 show the measured reflection coefficients for conducting plate sizes of 5" square and 12" square, respectively, when coated with Emerson and Cuming SF-9 material. The average midband material

parameters are $\varepsilon_r = (7.8, -j.17)$ and $\mu_r = (1.42, -j.8)$ with a thickness of .082". The plots also contain the calculated Fresnel reflection coefficient. Note that the measured response for larger plate size is off considerably since the far field condition is not met and the anticipated smaller return is obtained. These measured reflection coefficients were obtained from calibrated scattered fields using a 5" square conducting plate as a reference standard. The error shown in Figure 2.4 can be minimized if it is calibrated with a reference plate of the same size. All measurements employed vector background subtraction which entails the subtraction between measurements when a plate is present and absent.

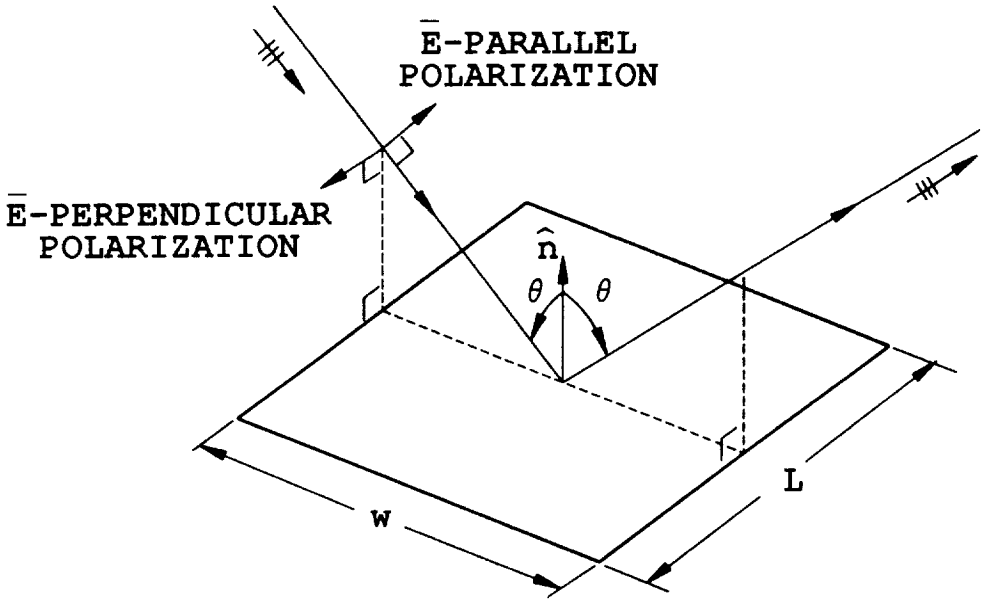

Figure 2.2: Far field scattering for a plate with plane wave incidence.

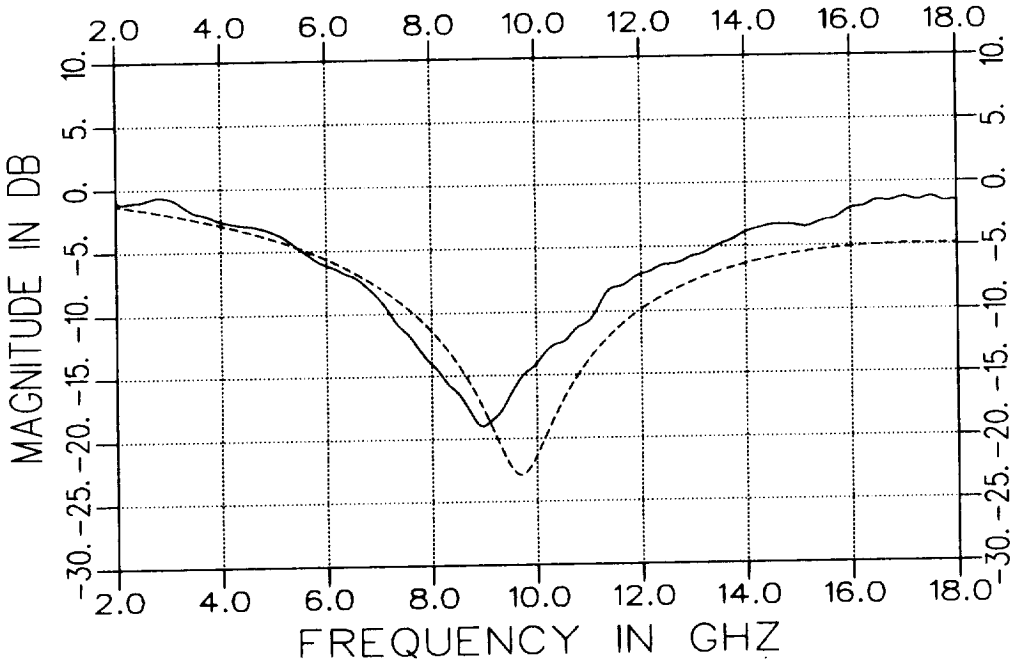

Figure 2.3: Measured (solid) and calculated (dashed) reflection coefficients for a 5" square planar sample of lossy magnetic material.

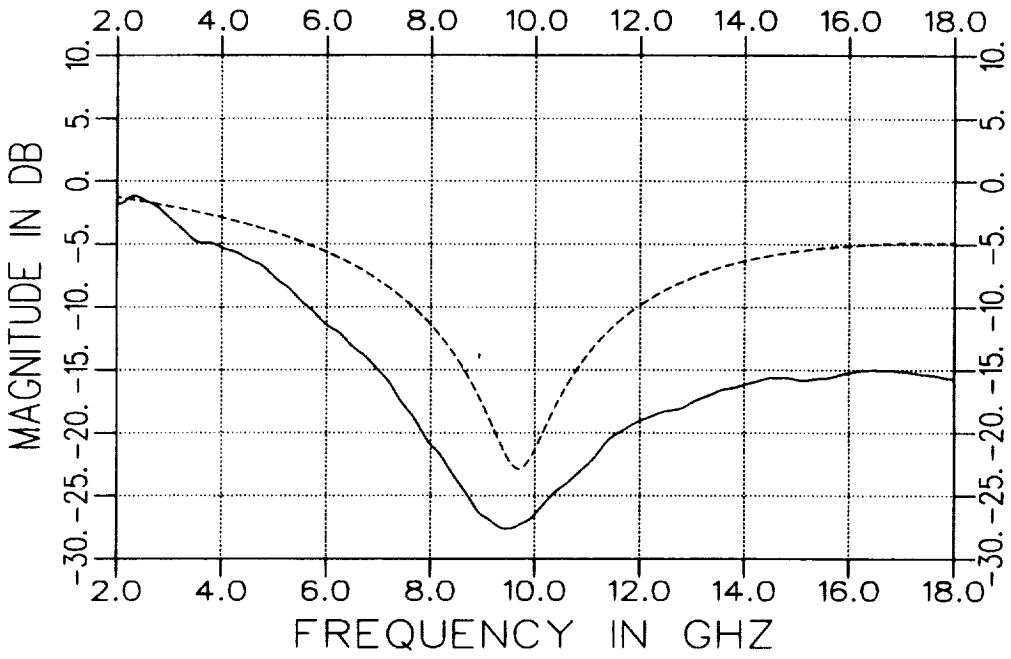

Figure 2.4: Measured (solid) and calculated (dashed) reflection coefficients for a 12" square planar sample of lossy magnetic material.

Chapter 3

Material Parameter Extraction Using Waveguides

A common approach for parameter determination is to obtain reflection and transmission measurements for a fixed length of material in a waveguide fixture (coaxial or rectangular) with the fixture cross section completely filled. The parameters extracted from such an approach are subject to error from sample condition (homogeneity, dimensions and shape distortions) and measurement hardware calibration. Examples of error magnitude will be presented for some of the errors. The error occured from an incompletely filled fixture cross section is presented in the following chapter. The basic equations used for such parameter extraction are presented here.

The measurements are facilitated with automated broadband network analyzers providing S_{11} (reflection) and S_{21} (transmission) characteristics for a sample length of d [5]. These measurements can be related to another set of reflection (Γ) and transmission (T) characteristics for a material junction semi-infinite length. The relationships are

$$S_{11} = \frac{(1 - T^2(\epsilon,\mu))\Gamma(\epsilon,\mu)}{(1 - T^2(\epsilon,\mu)\Gamma^2(\epsilon,\mu))} \tag{3.1}$$

and

$$S_{21} = \frac{(1 - \Gamma^2(\varepsilon,\mu))T(\varepsilon,\mu)}{(1 - T^2(\varepsilon,\mu)\Gamma^2(\varepsilon,\mu))}. \tag{3.2}$$

The previous expressions can be rewritten to express Γ and T in terms of S_{11} and S_{21}. These expressions are

$$T = \frac{S_{11} + S_{21} - \Gamma}{1 - (S_{11} + S_{21})\Gamma} \tag{3.3}$$

and

$$\Gamma = K \pm \sqrt{K^2 - 1} \tag{3.4}$$

where

$$K = \frac{S_{11}^2 - S_{21}^2 + 1}{2S_{11}}. \tag{3.5}$$

The sign in Equation (3.4) is chosen to insure $|\Gamma| \leq 1$.

These new characteristics, Γ and T, can be related to the material parameters. The relationships for a coaxial waveguide fixture are

$$T = e^{-j\frac{\omega}{c}\sqrt{\varepsilon_r\mu_r}d} \tag{3.6}$$

and

$$\Gamma = \frac{\sqrt{\frac{\mu_r}{\varepsilon_r}} - 1}{\sqrt{\frac{\mu_r}{\varepsilon_r}} + 1}. \tag{3.7}$$

Note that $\varepsilon = \varepsilon_r\varepsilon_o$ and $\mu = \mu_r\mu_o$ where the subscript notation refers to relative and free space values.

The corresponding relationships for a rectangular waveguide fixture are

$$T = e^{-j\frac{\omega}{c}X_1\sqrt{\epsilon_r\mu_r}d} \tag{3.8}$$

and

$$\Gamma = \frac{\sqrt{\frac{\mu_r}{\epsilon_r}}\frac{X_o}{X_1} - 1}{\sqrt{\frac{\mu_r}{\epsilon_r}}\frac{X_o}{X_1} + 1} \tag{3.9}$$

where $X_o = \sqrt{1-(\frac{\lambda_o}{2a})^2}$ and $X_1 = \sqrt{1-(\frac{\lambda_o}{2a\sqrt{\epsilon_r\mu_r}})^2}$ with λ_o being the free space wavelength, c the speed of light and a is the width of the rectangular guide.

The final expressions for the constitutive parameters using a coaxial waveguide are given by

$$\mu_r = \sqrt{xy} \tag{3.10}$$

and

$$\epsilon_r = \sqrt{\frac{y}{x}} \tag{3.11}$$

where

$$x = \left(\frac{1+\Gamma}{1-\Gamma}\right)^2 \tag{3.12}$$

and

$$y = -\left\{\frac{c}{\omega d}ln(\frac{1}{T})\right\}^2. \tag{3.13}$$

The final expressions for the constitutive parameters using a rectangular waveguide are given by

$$\mu_r = \frac{1+\Gamma}{1-\Gamma}\frac{\lambda_o}{\Lambda X_o} \tag{3.14}$$

and

$$\varepsilon_r = \left(\frac{1}{\Lambda^2} + \frac{1}{(2a)^2}\right)\frac{\lambda_o^2}{\mu_r} \tag{3.15}$$

where

$$\frac{1}{\Lambda^2} = -\left[\frac{1}{2\pi d} ln \frac{1}{T}\right]^2. \tag{3.16}$$

Note that $ln\frac{1}{T}$ is modulo $j2\pi n$ where n is the integer of $\frac{d}{\lambda_g}$. The proper value of n can be estimated with the integer value of

$$n = \text{Int}\left[\frac{f\Phi'}{2\pi}\right] \tag{3.17}$$

where Φ' is the derivative (slope) of the phase for the transmission coefficient T with respect to frequency and f is frequency.

An important aspect in parameter determination is the error occurred from calibration and sample dimensions. The following examples are for coaxial and rectangular waveguide fixtures with sample parameters of $\mu_r = (1.42, -j.8)$ and $\varepsilon_r = (7.8, -j.17)$ and a length of .05". Figures 3.1 and 3.2 illustrate error from the phase reference plane position for phase offsets in S_{11} corresponding to distances of .001" and .003", respectively. The error is defined as

$$\% \text{ Error} = \frac{\text{Extracted Value - Exact Value}}{\text{Exact Value}}. \tag{3.18}$$

The phase offset error (position) resulted in the same amount of error for both fixture types with the imaginary component of ε being very sensitive

to the position of the reference plane. Similar results also occur for the μ parameter.

Figures 3.3 and 3.4 illustrate the error when the sample length is assumed to be .048" and .052", respectively. The fixtures performed differently in this case with the coaxial fixture yielding a lower error than the rectangular waveguide fixture.

Other sources of error arise from other discontinuities occurring in the measurement system. The best solution so far has been to time gate the desired returns from the others which is readily performed with swept frequency measurements. It is also advisable to use a fixture with sufficient length to isolate the returns due to the fixture junctions from the sample return in the interior region of the fixture.

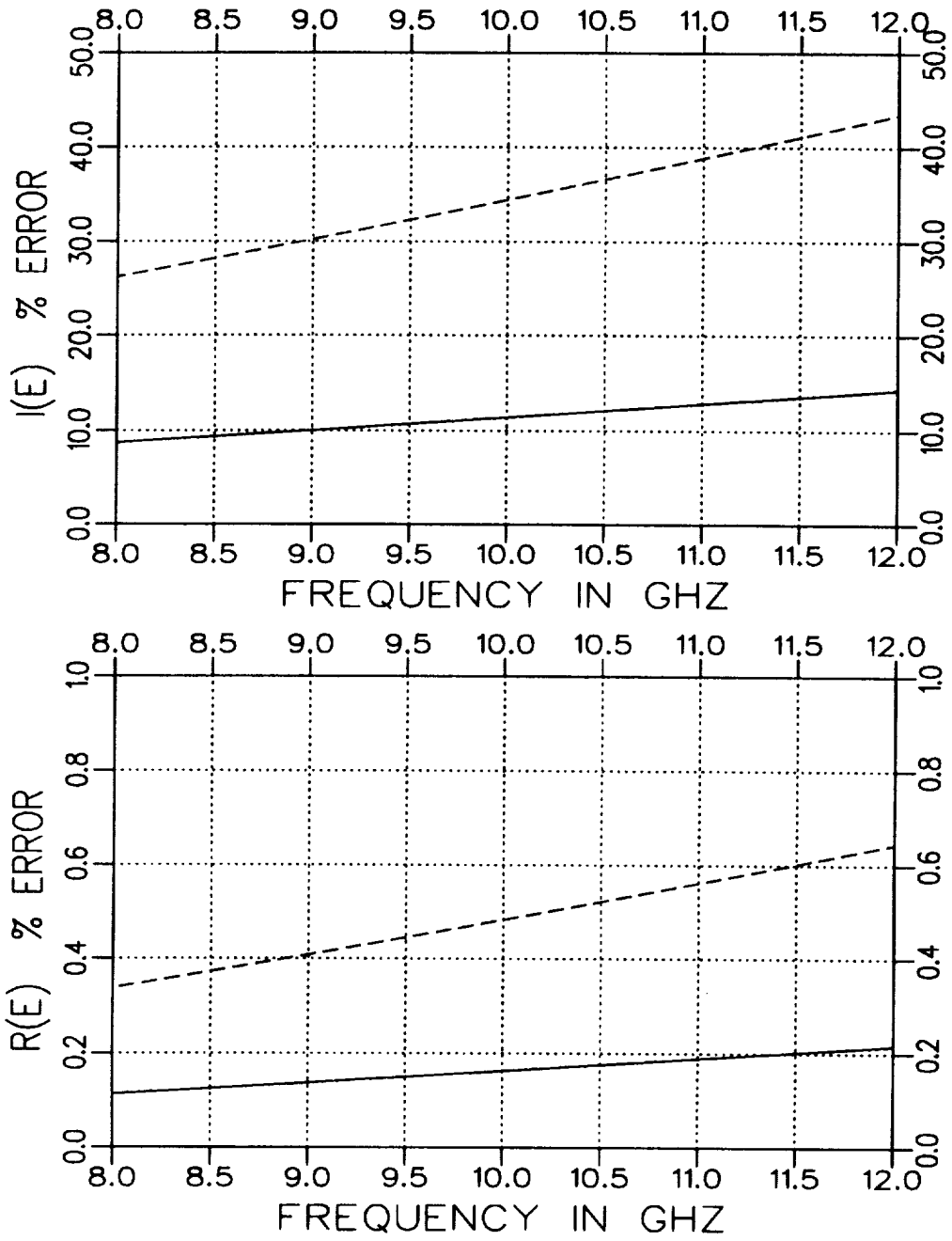

Figure 3.1: Normalized error for ε when S_{11} has a phase position error of .001" (solid) and .003" (dashed). The sample parameters are $\mu_r = (1.42, -j.8)$ and $\varepsilon_r = (7.8, -j.17)$ with $d = .05$". Coaxial airline fixture.

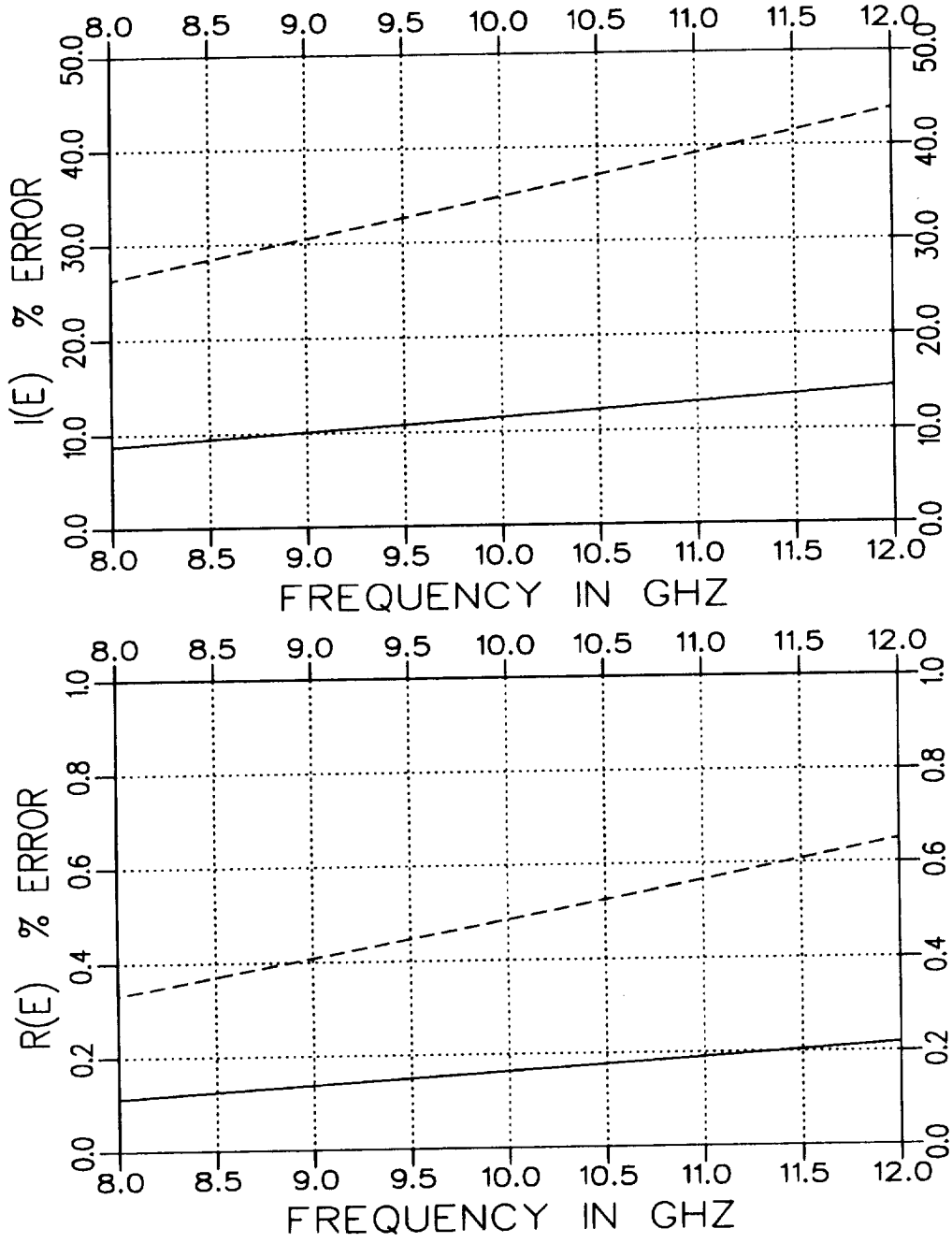

Figure 3.2: Normalized error for ϵ when S_{11} has a phase position error of .001" (solid) and .003" (dashed). The sample parameters are $\mu_r = (1.42, -j.8)$ and $\epsilon_r = (7.8, -j.17)$ with $d = .05$". Rectangular waveguide fixture.

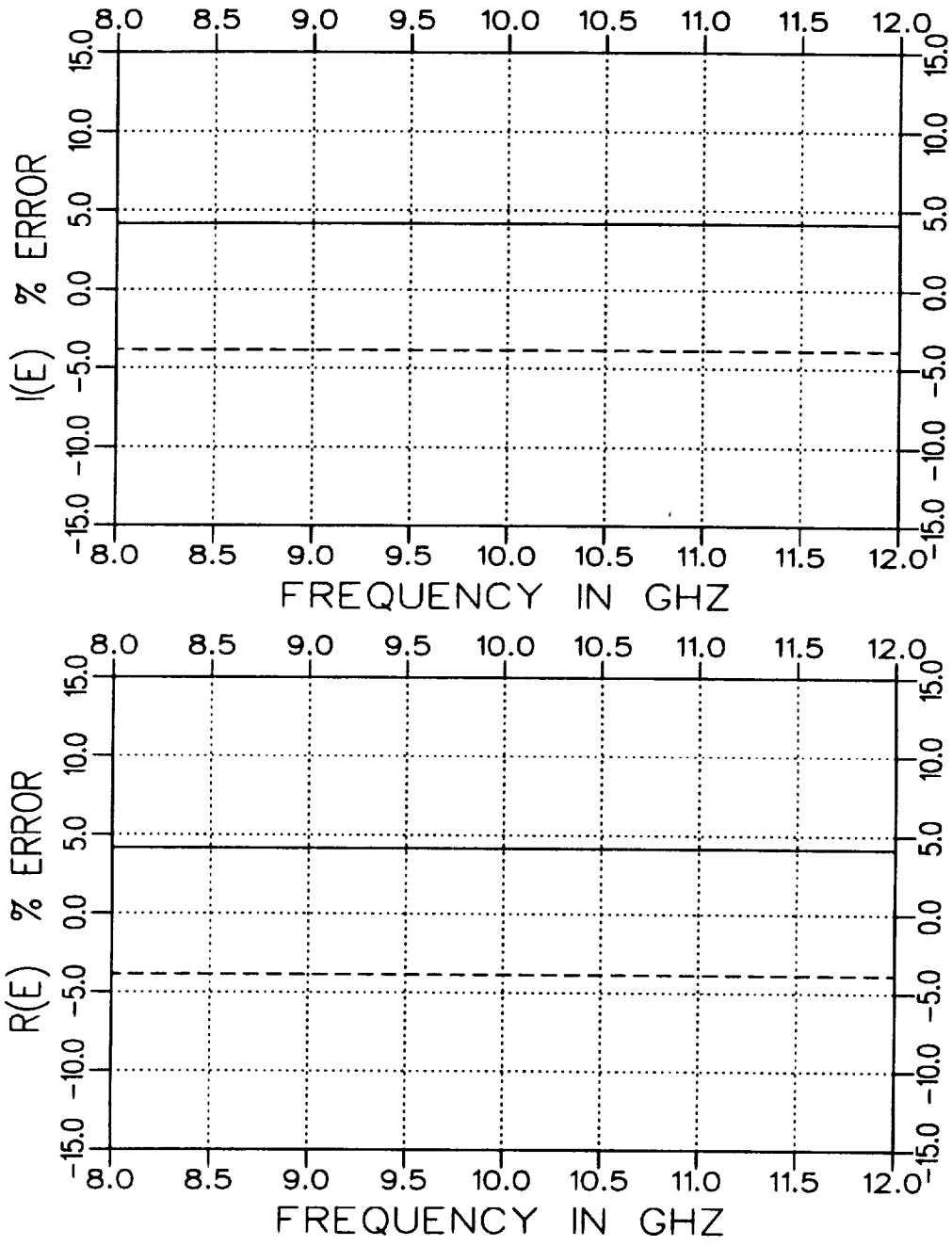

Figure 3.3: Normalized error for ϵ when S_{11} has a sample length error of $-.002$" (solid) and $+.002$" (dashed). The sample parameters are $\mu_r = (1.42, -j.8)$ and $\epsilon_r = (7.8, -j.17)$ with $d = .05$". Coaxial airline fixture.

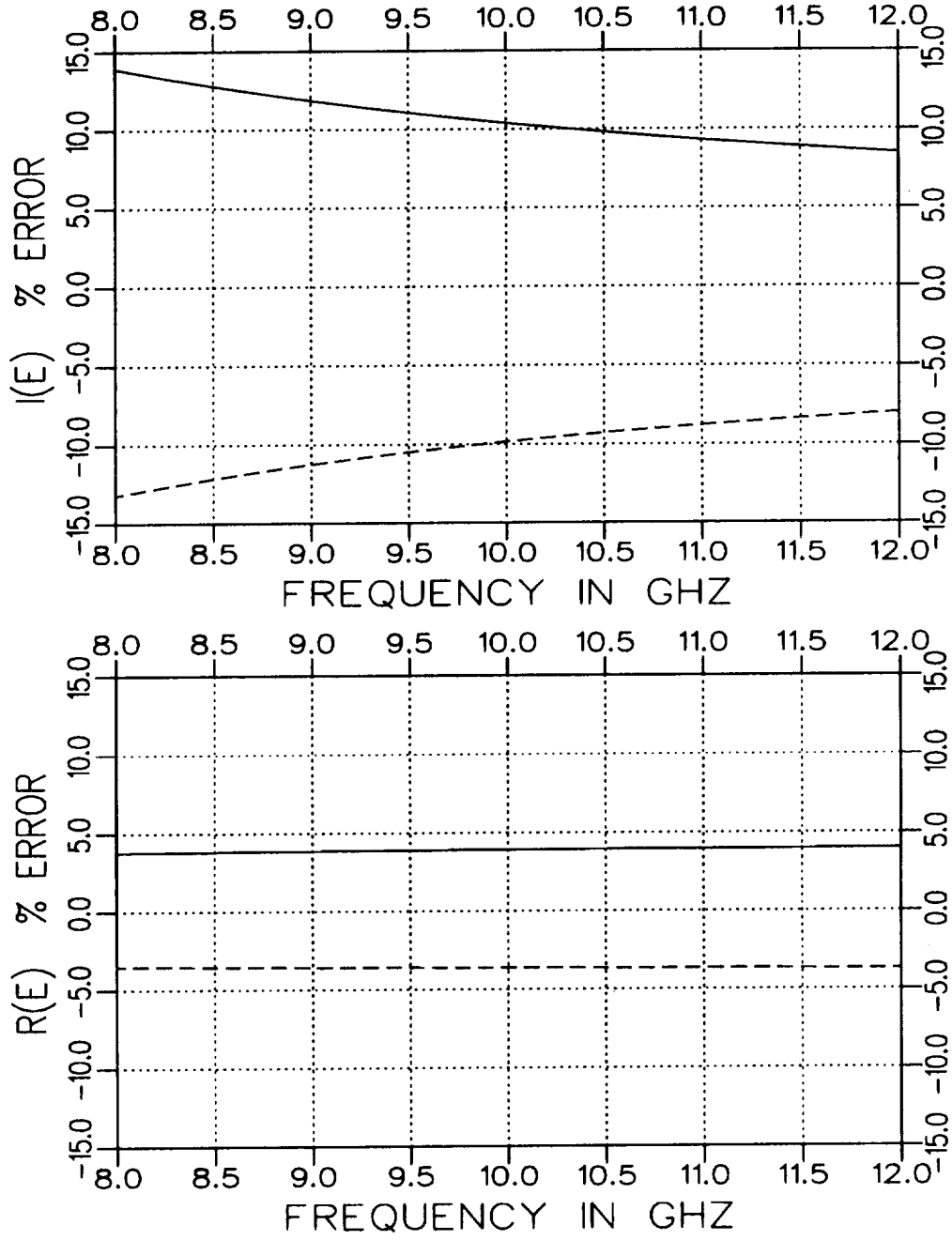

Figure 3.4: Normalized error for ε when S_{11} has a sample length error of $-.002$" (solid) and $+.002$" (dashed). The sample parameters are $\mu_r = (1.42, -j.8)$ and $\varepsilon_r = (7.8, -j.17)$ with $d = .05$". Rectangular waveguide fixture.

Chapter 4

Partially Filled Waveguides

An accurate parameter extraction using a waveguide fixture with a cross section completely filled with material requires that no air gaps exist between the material and the walls of the waveguide. It is believed that the tolerance of the dimensions of a material sample can be relaxed if the field solution has a defined air gap. Any slight changes due to sample dimension error or temperature expansion will not dramatically impact the measured quantities as significantly as if no air gap is to be present.

The geometries under consideration are shown in Figure 4.1. Geometry B for the rectangular waveguide is more desirable than Geometry A since a small air gap along the short wall length is not as critical as along the longer wall length due to the electric field direction of the excitation field.

The disadvantage for such a sample geometry presents itself in actually acquiring the material parameters. The S_{11} and S_{21} parameters have a complicated analytical representation which involve a moderate amount of numerical calculation to obtain. Hence, explicit expressions are not available to obtain ϵ and μ. The parameters ϵ and μ have to be obtained through a numerical Newton-Raphson search. The search involves iterating on ϵ and

μ until the following two functionals are driven to zero:

$$F_1 = S_{11}^{cal} - S_{11}^{meas} \tag{4.1}$$

$$F_2 = S_{21}^{cal} - S_{21}^{meas}. \tag{4.2}$$

The calculation of S_{11} and S_{21} involves the modal expansion of the fields in all three regions and performing a modal matching at the material interfaces ($z = 0$ and $z = d$) for the geometry shown in Figure 4.2 [6]. The modal matching is essentially a three dimensional method of moments solution using entire basis functions. The modal matching at the two interfaces were reduced to just one interface using a self-consistent approach. The required S_{11} and S_{21} can be related to another set of scattering parameters for a semi-infinite geometry as shown in Figure 4.2. The relationships between these parameters are

$$S_{11} = \left\{ [s_{11}] + [s_{12}][P][s_{22}][P] \left[[I] - [s_{22}][P][s_{22}][P] \right]^{-1} [s_{21}] \right\} \tag{4.3}$$

and

$$S_{21} = [s_{12}][P] \left[[I] - [s_{22}][P][s_{22}][P] \right]^{-1} [s_{21}]. \tag{4.4}$$

The variables s_{ij} are the modal scattering matrices for the semi-infinite geometry and $[P]$ is the modal propagation matrix corresponding to length d.

I Field Expansions

The required elements for the scattering matrices $[s_{ij}]$ are obtained through a modal matching technique for the field expansions in both regions. The

tangential field matching yields expansion coefficients for the expansion modes. The expansion modes for the Geometry A in a rectangular fixture are given below.

Region I

$$E_y = (e^{-\Gamma_1 z} + a_1 e^{\Gamma_1 z})\Phi_1 + \sum_{n=2}^{\infty} a_n \Phi_n e^{\Gamma_n z} \tag{4.5}$$

and

$$H_x = -Y_1(e^{-\Gamma_1 z} - a_1 e^{\Gamma_1 z})\Phi_1 + \sum_{n=2}^{\infty} a_n Y_n \Phi_n e^{\Gamma_n z} \tag{4.6}$$

where

$$\Phi_n = \sqrt{\frac{2}{a}} \sin \frac{n\pi}{a} x, \tag{4.7}$$

$$\Gamma_n^2 = \left(\frac{n\pi}{a}\right)^2 - k_o^2 \quad \text{and} \tag{4.8}$$

$$Y_n = \frac{\Gamma_n}{jZ_o k_o}. \tag{4.9}$$

Region II

$$E_y = \sum_{n=1}^{\infty} b_n \Psi_n e^{-\gamma_n z} \tag{4.10}$$

and

$$H_x = -\sum_{n=1}^{\infty} b_n Y_{in} \Psi_n e^{-\gamma_n z} \tag{4.11}$$

where

$$\begin{array}{ll} \Psi_n = C \sin k_{x_{1n}} x & \text{for } 0 \le x \le d, \\ \Psi_n = C \frac{\sin k_{x_{1n}} d}{\sin k_{x_{0n}}(a-d)} \sin k_{x_{0n}}(a-x) & \text{for } d \le x \le a, \\ \gamma_n^2 = k_{x_{1n}}^2 - k_o^2 \varepsilon_r \mu_r = k_{x_{0n}}^2 - k_o^2, & \\ Y_{1n} = \frac{\gamma_n}{jZ_o k_o \mu_r} & \text{for } 0 \le x \le d, \\ Y_{0n} = \frac{\gamma_n}{jZ_o k_o} & \text{for } d \le x \le a \end{array} \tag{4.12}$$

and C is a normalization constant.

Comparable field expansions are required for the other geometries but are not presented here for simplicity. The unknown coefficients are then obtained by solving for them with following expression

$$\int_{z=0^-} \mathbf{E} \times \mathbf{H} dS = \int_{z=0^+} \mathbf{E} \times \mathbf{H} dS \tag{4.13}$$

through generating a system of equations from a method of moments approach using entire bases testing functions.

II Calculations and Measurements

Software only for the rectangular Geometry A has been completed as of now. Figures 4.3 and 4.4 illustrate S_{11} and S_{21} for $t = .2", .5", .7"$, and .9" in a X-band fixture (.4"x.9") when $\mu_r = (1.42, -j.8)$, $\varepsilon_r = (7.8, -j.17)$ and $l = .3"$. The variation of S_{11} and S_{21} decreases rapidly as the guide becomes completely filled which indicates a small air gap to the short wall may not be that critical.

Figures 4.5 and 4.6 illustrate S_{11} and S_{21} for $\varepsilon_r = 2, 5, 8, 11$, and 14 in a X-band fixture (.4"x.9") when $\mu_r = (1., -j0.)$, $t = .1"$ and $l = .5"$. The variation of S_{11} is quite sensitive for any loading and S_{21} would show more variation if loss was present in the sample.

Figure 4.7 illustrates the error in extracting the parameters assuming the cross section of the waveguide is completely filled but actually having an air gap. The air gap was .002" with $\mu_r = (1.42, -j.8)$, $\varepsilon_r = (7.8, -j.17)$ and $l = .3"$. As anticipated, the error is very small since the electric field in the air gap is parallel to a conducting boundary and hence is very small.

The error shown is comparable to the results when the fixture is completely filled giving an indication of the accuracy of the calculation.

Figures 4.8 and 4.9 illustrate the comparison of the measured and calculated S_{11} and S_{21} parameters for a X-band waveguide shown in Figure 4.10. The sample dimensions were $t = .082$" and $l = .9$". The calculated response used estimated parameters of $\mu_r = (1.42, -j.8)$ and $\varepsilon_r = (7.8, -j.17)$. The comparison is good and any differences can be attributed to the estimated parameters used in the calculations. The parameter estimates were "average" values obtained from coaxial fixture measurements.

Comparable results for the rectangular waveguide Geometry B have not been obtained yet. Figures 4.11 and 4.12 are measured results for the rectangular waveguide Geometry B for comparison purposes to the Geometry A results.

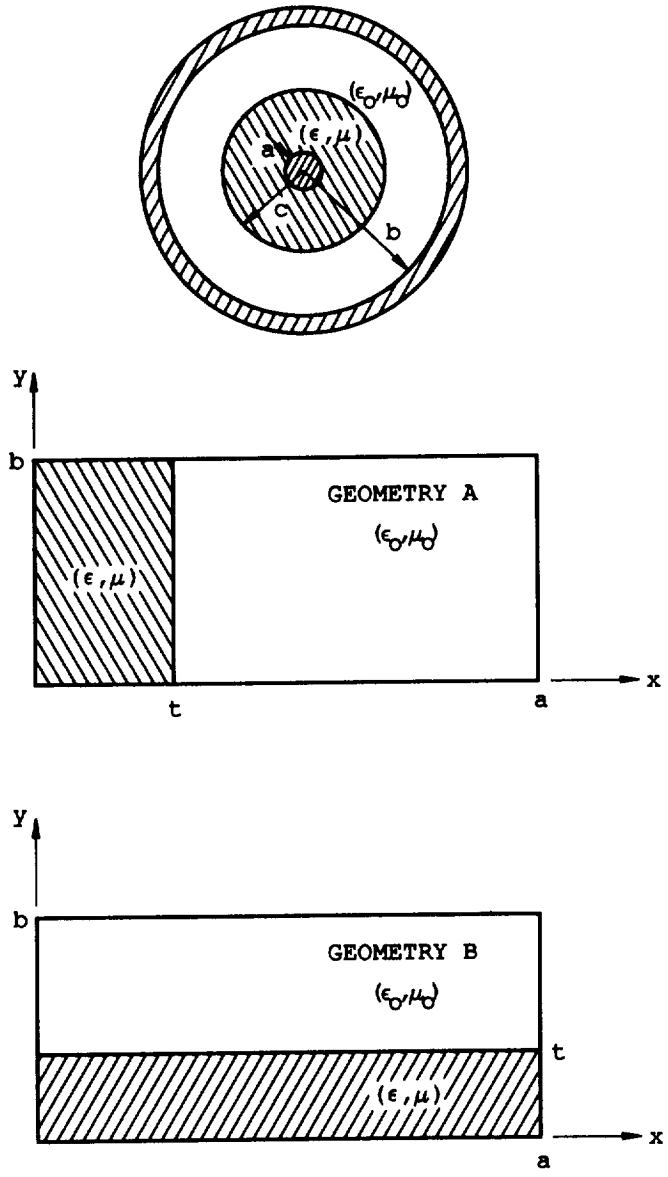

Figure 4.1: Partially filled waveguide geometries.

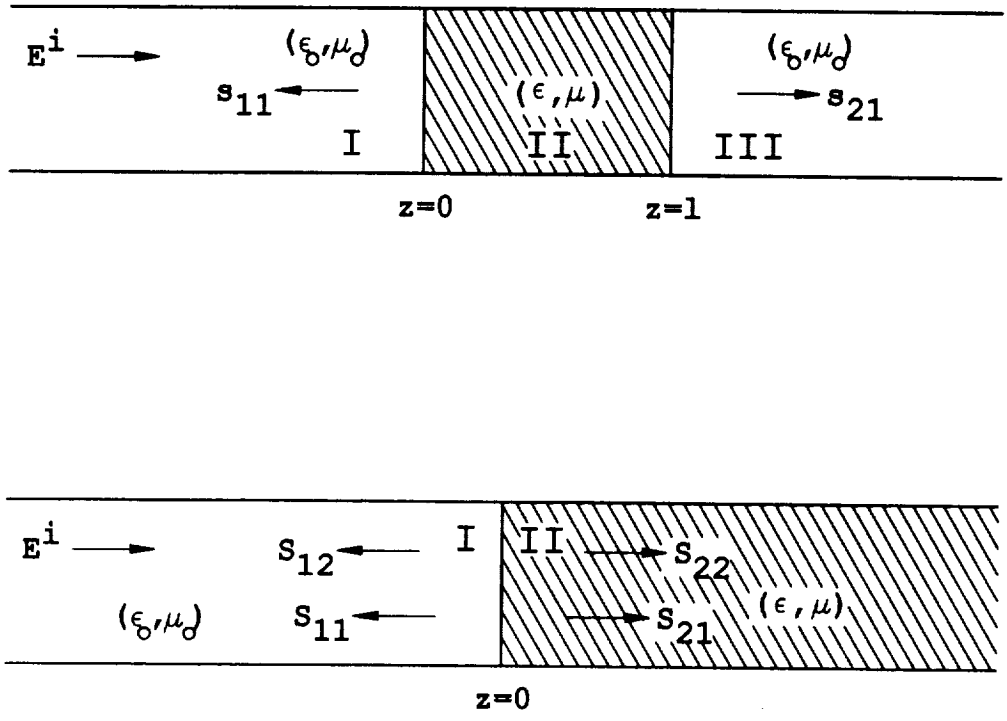

Figure 4.2: Waveguide regions.

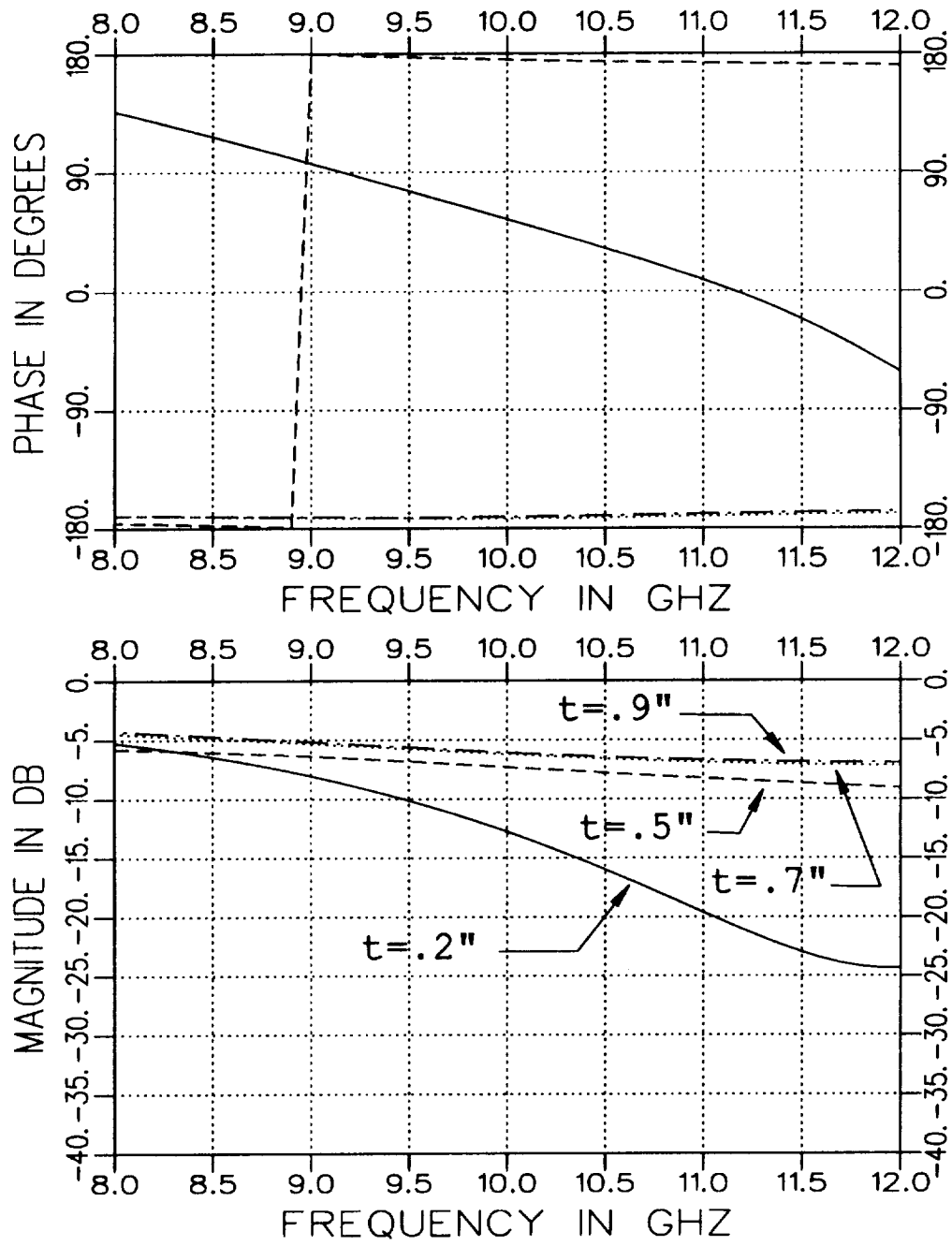

Figure 4.3: Calculated S_{11} for $t = .2", .5", .7"$, and $.9"$ in a X-band fixture ($.4"$x$.9"$) when $\mu_r = (1.42, -j.8)$, $\varepsilon_r = (7.8, -j.17)$ and $l = .3"$.

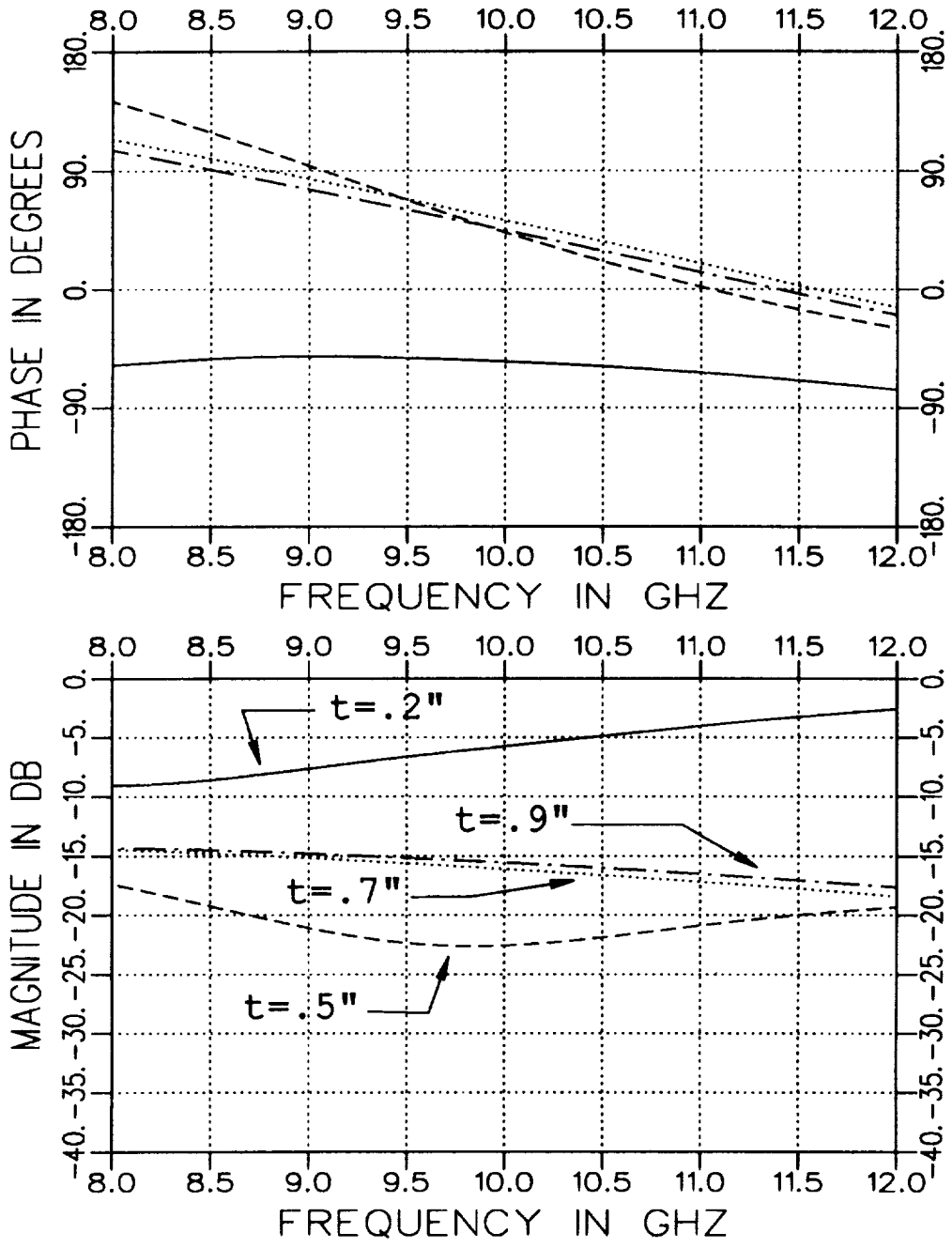

Figure 4.4: Calculated S_{21} for $t = .2", .5", .7"$, and $.9"$ in a X-band fixture (.4"x.9") when $\mu_r = (1.42, -j.8)$, $\epsilon_r = (7.8, -j.17)$ and $l = .3"$.

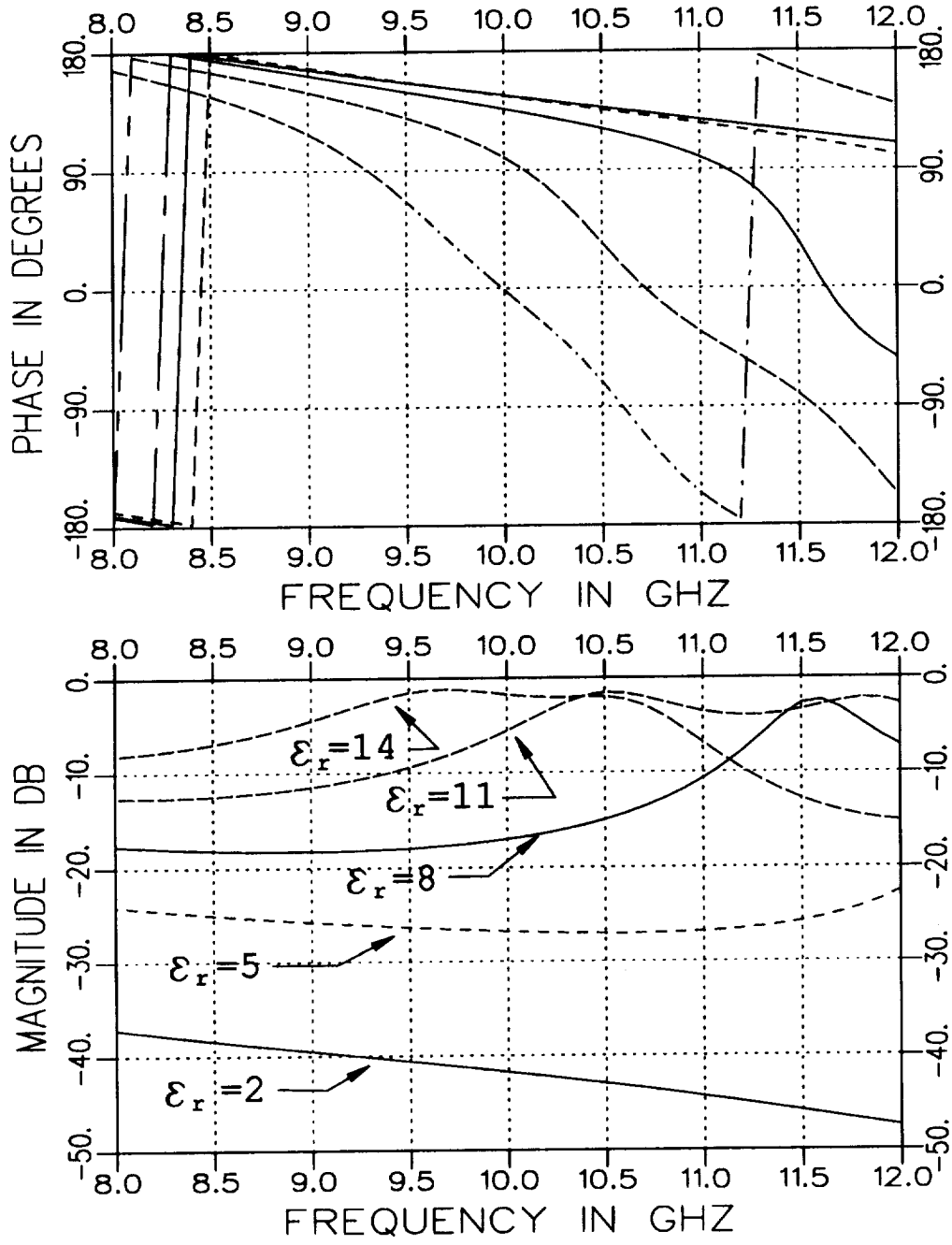

Figure 4.5: Calculated S_{11} for $\varepsilon_r = 2, 5, 8, 11$, and 14 in a X-band fixture (.4"x.9") when $\mu_r = (1., -j0.)$, $t = .1$" and $l = .5$".

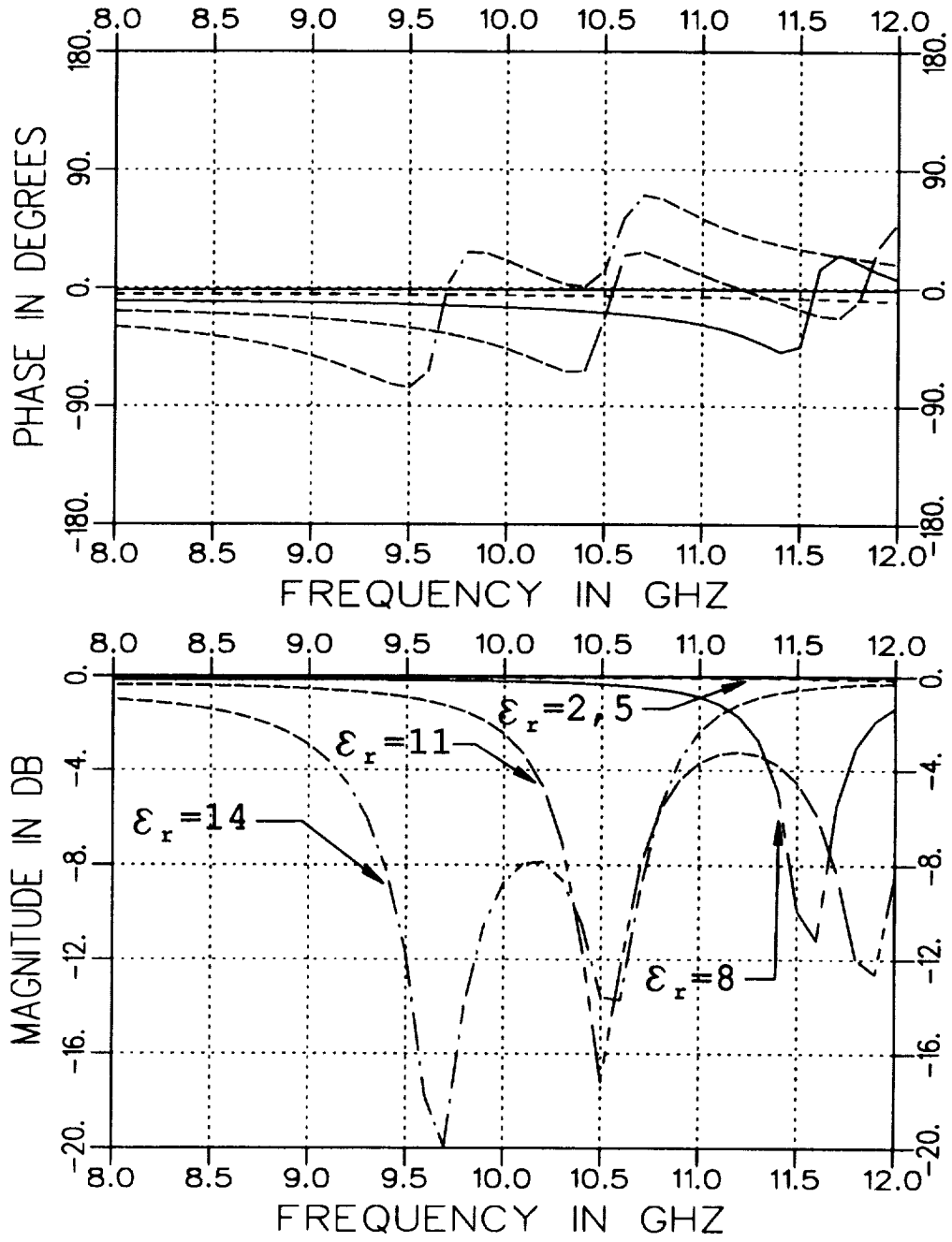

Figure 4.6: Calculated S_{21} for $\varepsilon_r = 2, 5, 8, 11$, and 14 in a X-band fixture (.4"x.9") when $\mu_r = (1., -j0.)$, $t = .1$" and $l = .5$".

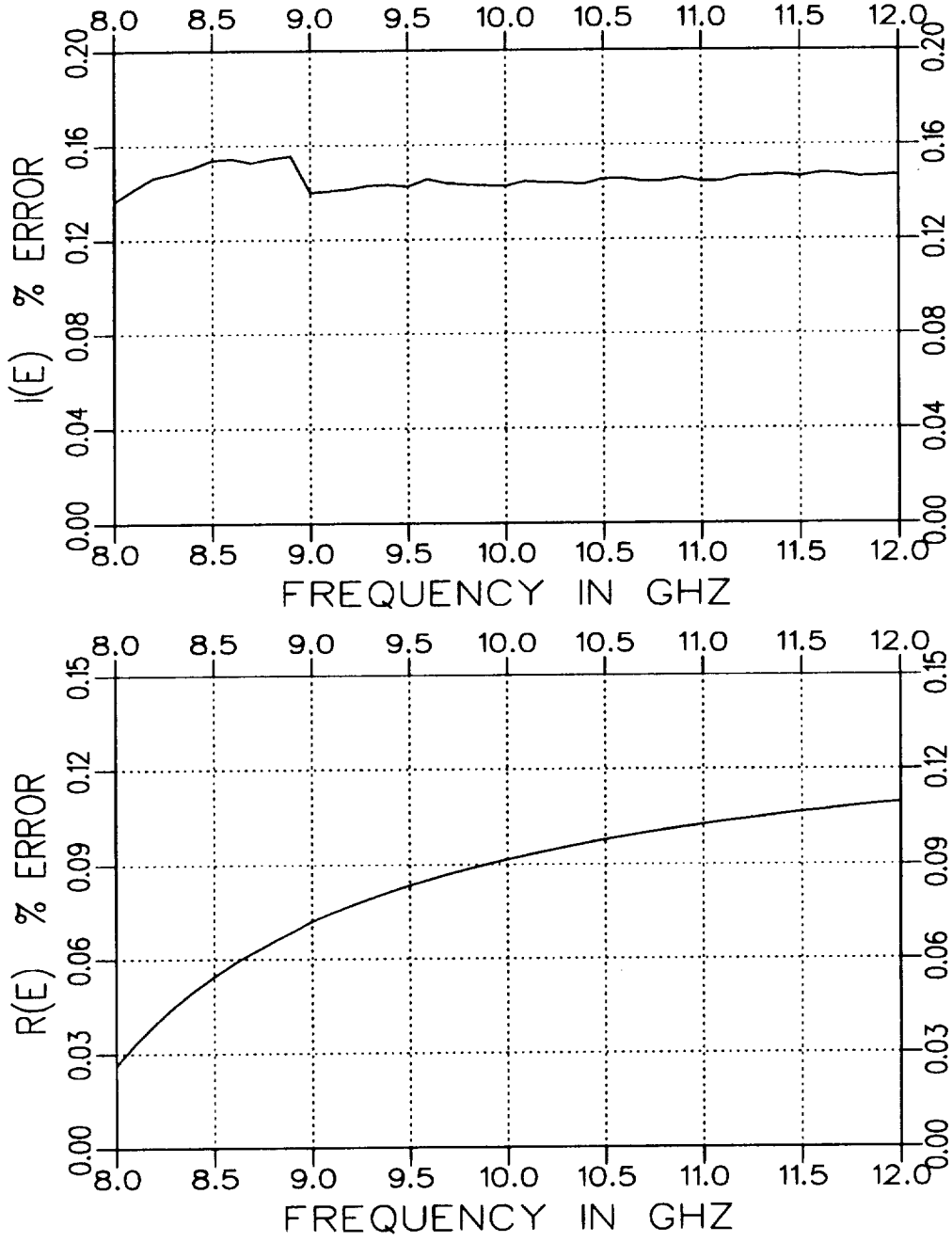

Figure 4.7: Calculated error for a .002" air gap along the short wall for a rectangular guide with $\mu_r = (1.42, -j.8)$, $\epsilon_r = (7.8, -j.17)$ and $l = .3$".

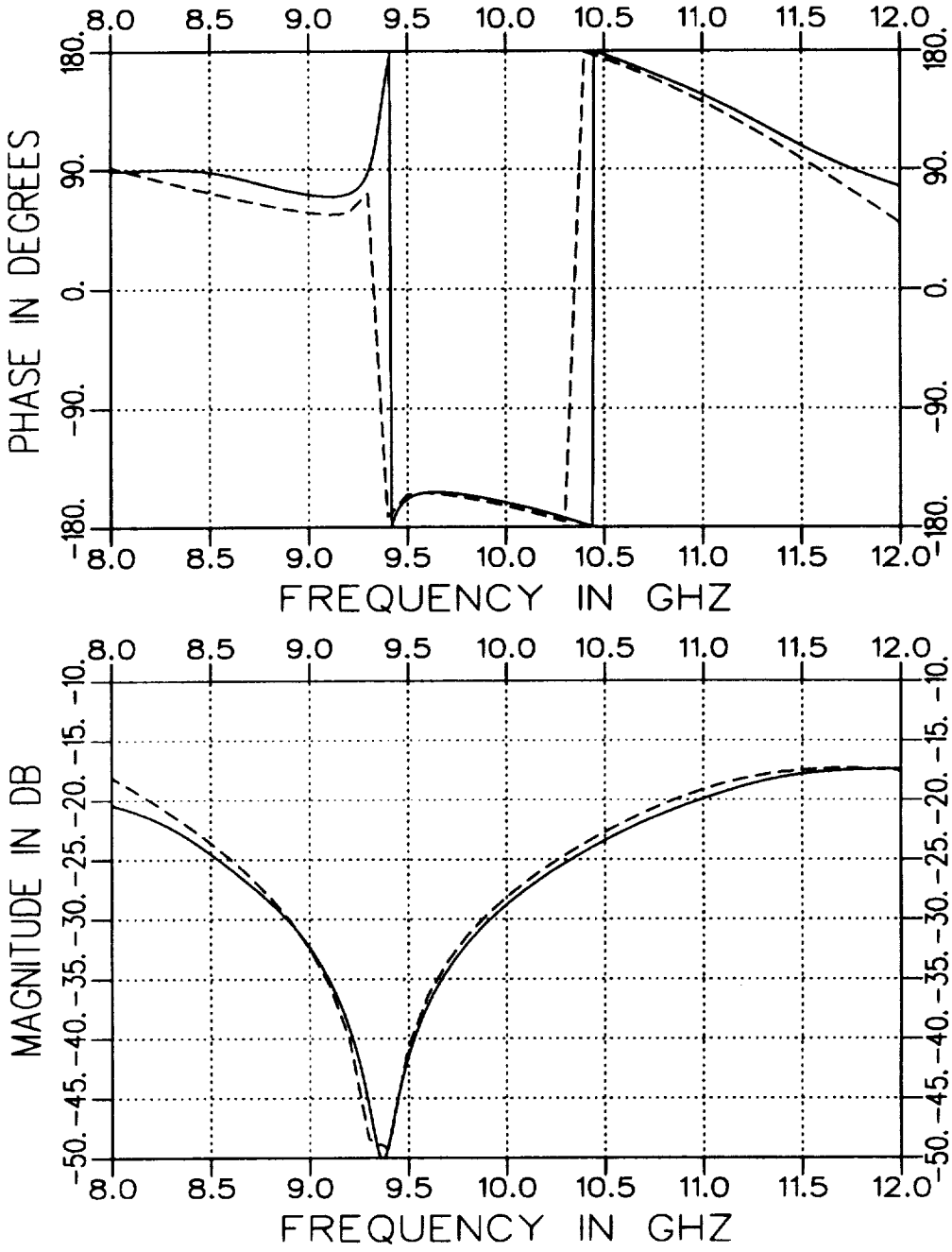

Figure 4.8: Measured and calculated S_{11} for a partially filled rectangular X-band guide with $t = .082$". Geometry A.

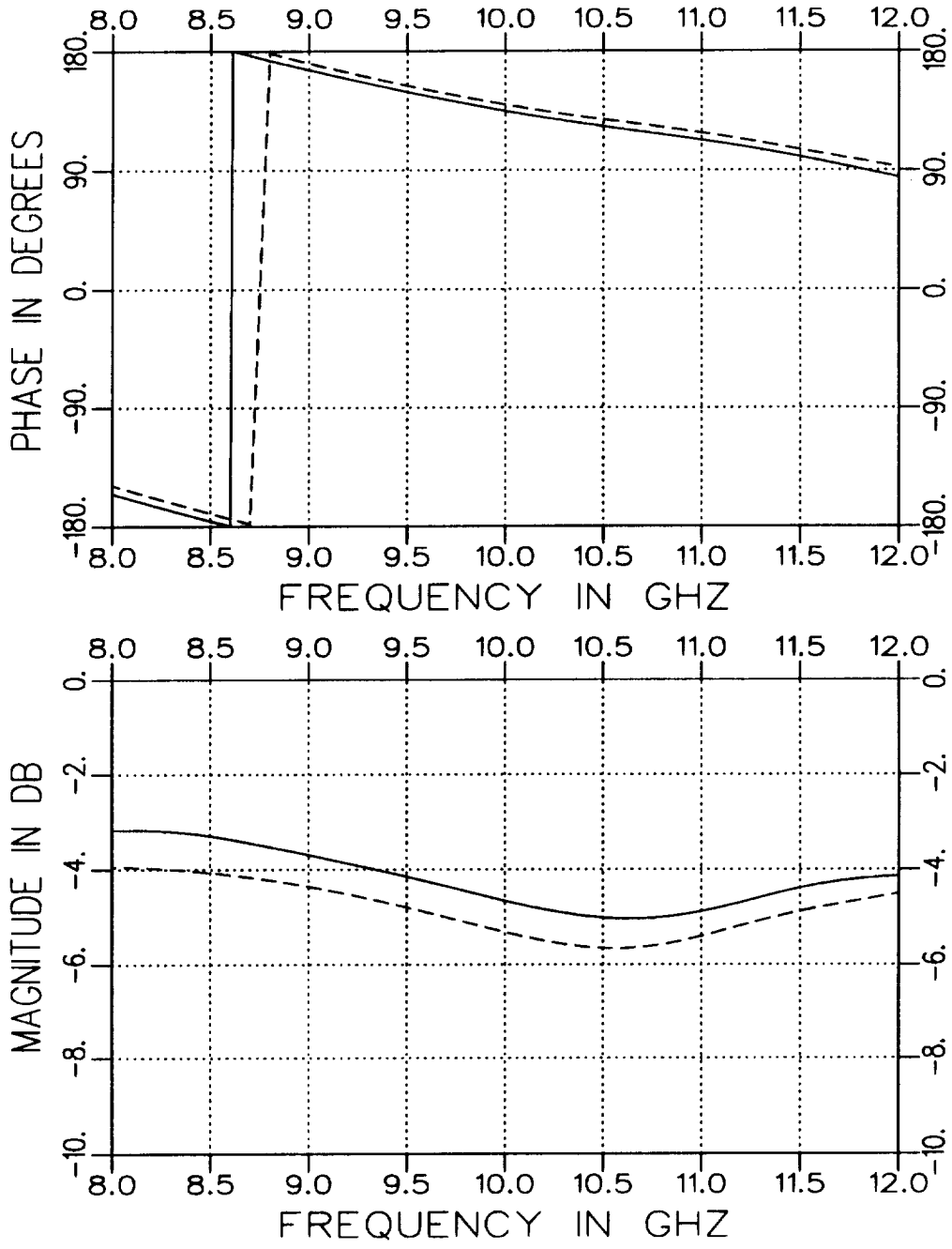

Figure 4.9: Measured and calculated S_{21} for a partially filled rectangular X-band guide with $t = .082$". Geometry A.

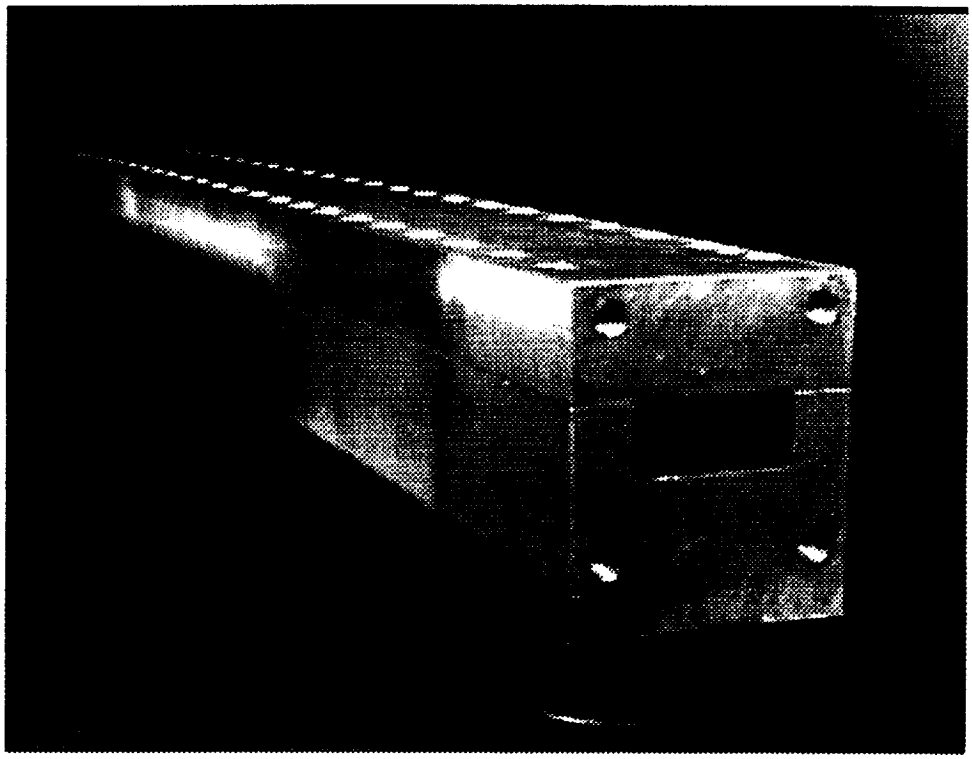

Figure 4.10: Illustration of X-band fixture used for material measurements.

ORIGINAL PAGE
BLACK AND WHITE PHOTOGRAPH

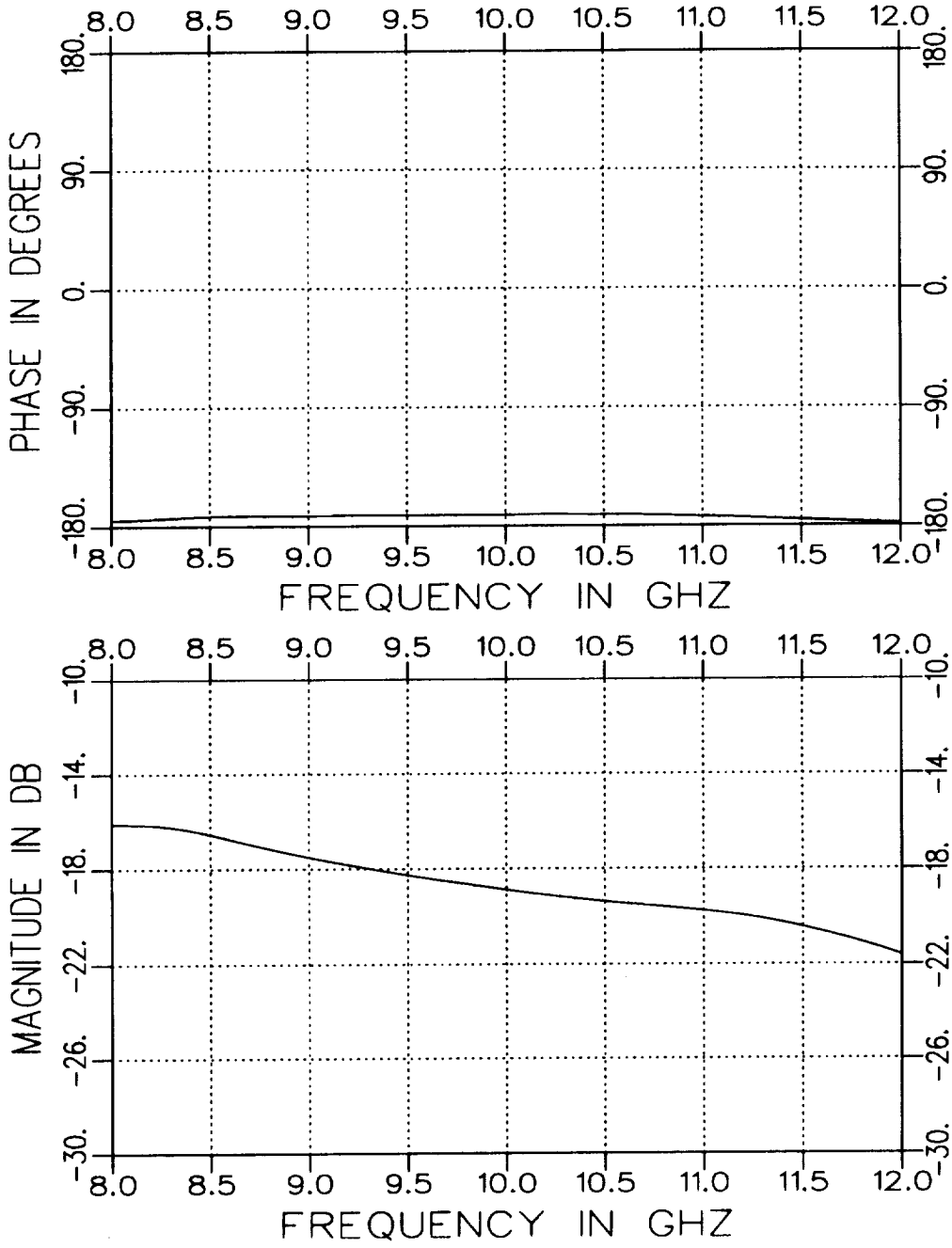

Figure 4.11: Measured S_{11} for a partially filled rectangular X-band guide with $t = .082$". Geometry B.

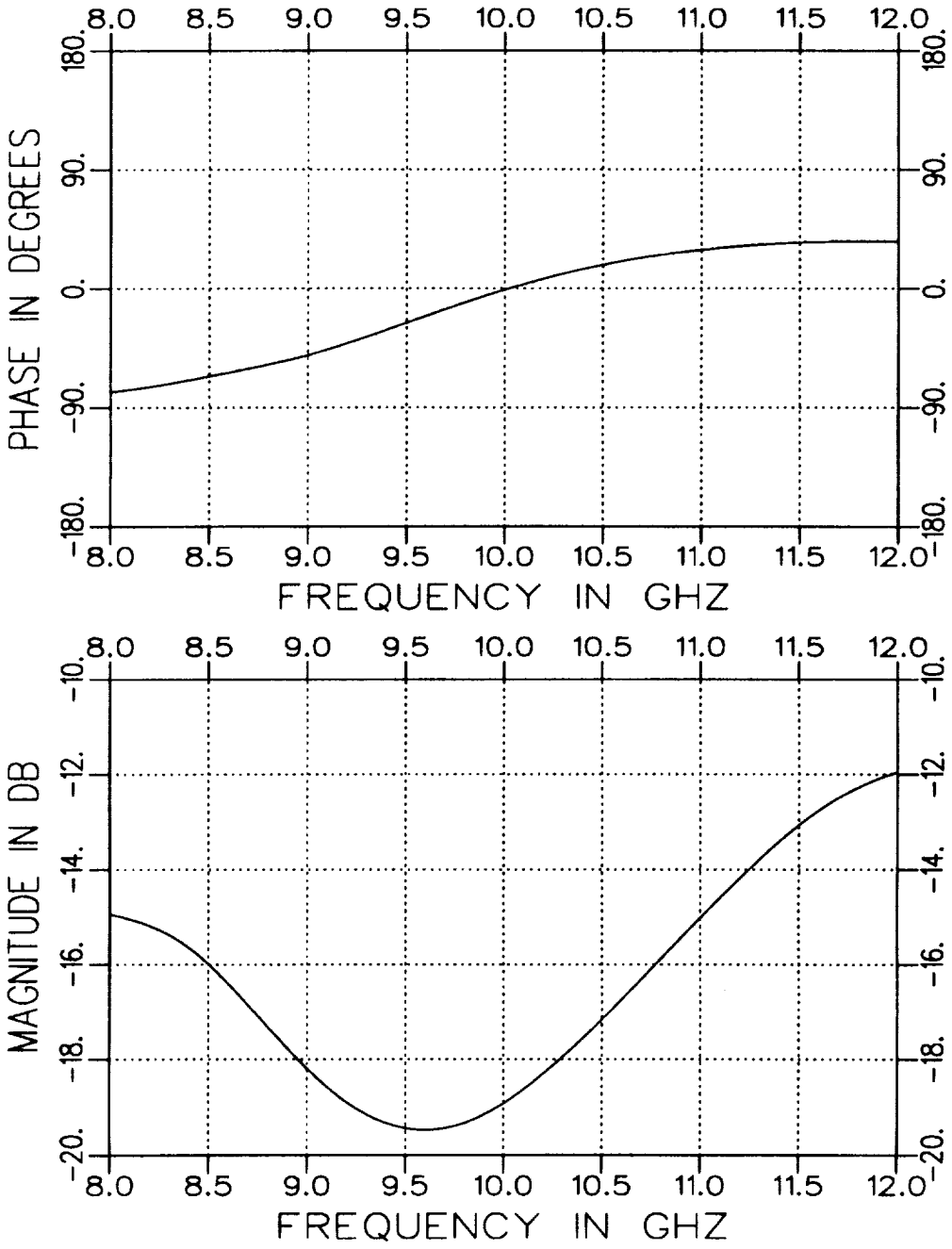

Figure 4.12: Measured S_{21} for a partially filled rectangular X-band guide with $t = .082$". Geometry B.

Chapter 5

Conclusions

The major focus for this work has been to examine alternate sample geometries to relax the required tolerances on sample dimensions for elevated temperature measurements. The numerical effort for the partially filled fixture is considerable more than the completely filled fixture. The numerical solution for the other geometries are presently being generated. It is expected that an air gap for the other geometries will be more critical due to the gap orientation and electric field direction. The most appropriate partially filled geometry for parameter extraction will be found based upon numerical effort and final fixture considerations for elevated temperature measurements.

Bibliography

[1] R. Torres, "Near Field and Far Field Scattering from a Strip Using the Geometrical Theory of Diffraction," Master's Thesis, Electrical Engineering Department, The Ohio State University, 1986.

[2] W. Burnside and K Burgener, "High Frequency Scattering by a Thin Lossless Dielectric Slab," IEEE Trans. on Antennas and Propagation, pp. 104-119, January 1983.

[3] A. Dominek, "A Material Sample Scattering Analysis for an NRL Arch," Oral Presentation, 10th Annual Conference, Antenna Measurement Techniques Association, Atlanta, GA, September 1988.

[4] D. Ghodgaonkar, V.V. Varadan, V.K. Varadan, "A New Free-Space Method for Explicit Determination of Complex Permittivity and Complex Permeability of Magnetic Materials at Microwave Frequencies using Bistatic Measurements," IEEE AP Symposium and URSI Meeting, San Hose, 1989.

[5] HP Product Note 8510-3, "Measuring Dielectric Constant with the HP 8510 Network Analyzer," Hewlett-Packard.

[6] R. Harrington, Time Harmonic Electromagnetic Waves, McGraw-Hill Company, New York, NY, 1961.